Adaptive Temperature Control of Air Conditioners Based on Millimeter-Wave Radar and Light Gradient Boosting Machine Model

Yunlong Xia , Zuoting Song , Wanna Zhang , Zhe Shang , Zhuoqi Zeng * , Amr Alanwar *

Posted Date: 19 May 2026

doi: 10.20944/preprints202605.1281.v1

Keywords: millimeter-wave radar; bed localization; air conditioning; adaptive temperature control; LGBM; temperature fluctuation suppression; thermal comfort

 doi:10.20944/preprints202605.1281.v1

Article

Adaptive Temperature Control of Air Conditioners Based on Millimeter-Wave Radar and Light Gradient Boosting Machine Model

Yunlong Xia [1,2,3], Zuoting Song [2,3], Wanna Zhang [2,3], Zhe Shang [2,3], Zhuoqi Zeng [4,*] and Amr Alanwar [1,*]

[1] Technical University of Munich, Munich, 80333, Germany
[2] Midea Group, Shanghai, 200000, China
[3] Shanghai Nearlink Open Lab, Shanghai, 200000, China
[4] Hainan Bielefeld University of Applied Sciences, Haikou, 570100, China
* Correspondence: zhuoqi.zeng@hainan-biuh.edu.cn (Z.Z.); alanwar@tum.de (A.A.)

Highlights

- A bed localization algorithm using millimeter-wave radar point cloud clustering is proposed, achieving 83.6% accuracy under 0.5 m error tolerance across 719 real devices.
- An LGBM weak teacher model is constructed to optimize air direction and speed, reducing the return air temperature fluctuation to 0.21°C with a control accuracy of the air guide mechanism over 0.98.
- The proposed method enables high-precision adaptive temperature control without hardware modification, featuring low cost, strong universality, and improved thermal comfort for bedroom air conditioners.

Abstract

To address the issues of large temperature fluctuations, poor spatial perception, and low control robustness in traditional residential air conditioners, this paper proposes an adaptive temperature control algorithm based on millimeter-wave radar and a Light Gradient Boosting Machine (LGBM). Given that the bed is the primary obstacle and heat source in a bedroom, we develop a bed localization method using point cloud clustering. This method accurately identifies the bed position through time-window filtering, outlier removal, and density clustering. An LGBM weak teacher model, trained on massive cloud data, takes the bed position, indoor temperature, and compressor parameters as inputs to optimize air direction and fan speed, thereby effectively suppressing steady-state fluctuations in the return air temperature. Experiments on 719 real-world devices demonstrate that the bed positioning accuracy reaches 83.6% under an error tolerance of 0.5 m, the average absolute temperature fluctuation is reduced to 0.21°C, and the control accuracy of the air guide mechanism exceeds 0.98. The proposed method requires no hardware modification, offers strong generalizability and low deployment cost, significantly improves temperature stability and thermal comfort in bedroom environments, and provides a feasible technical solution for intelligent residential air conditioning control.

Keywords: millimeter-wave radar; bed localization; air conditioning; adaptive temperature control; LGBM; temperature fluctuation suppression; thermal comfort

1. Introduction

Air conditioning is an indispensable component in modern buildings, which enables control over indoor air temperature, humidity, airflow velocity, and direction to provide a satisfactory thermal environment for occupants [1]. As one of the most energy-intensive electrical systems in buildings,

 doi:10.20944/preprints202605.1281.v1

the operating mode of air conditioners directly affects building energy efficiency, as well as indoor thermal comfort and work efficiency [2,3].

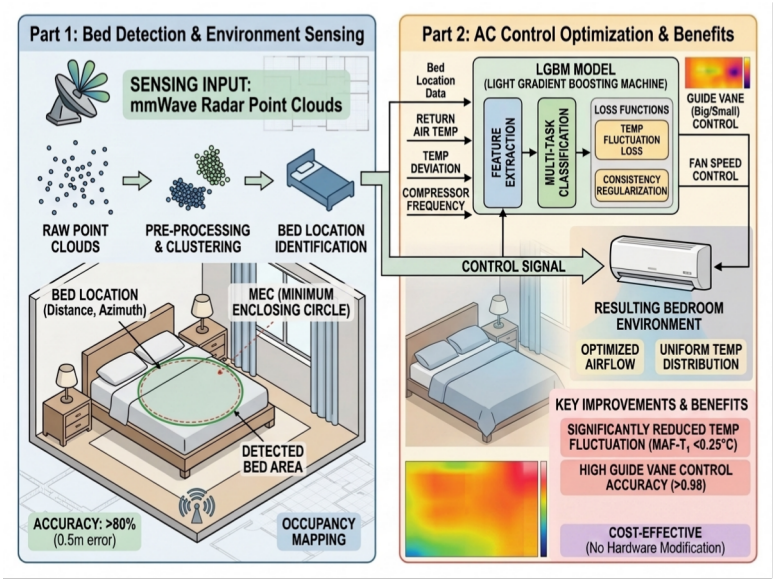

Figure 1. Workflow of mmWave radar-based bed detection and AC control. Bed location is identified via point cloud clustering, and an LGBM model enables multi-task control of guide vane and fan speed, achieving uniform temperature model.

According to compressor control strategies, air conditioners are classified into fixed-frequency and variable-frequency types. Fixed-frequency air conditioners adopt fixed-speed compressors and regulate temperature by switching the compressor on and off [4]. This operation leads to large indoor temperature fluctuations, compromising both comfort and energy efficiency. Due to operational limitations, fixed-frequency air conditioners are mostly applied in small spaces with limited budgets, short-term usage, or stable thermal loads [5,6]. Variable-frequency air conditioners use inverters to convert grid-frequency alternating current into adjustable-frequency power supplies, enabling dynamic matching of cooling or heating capacity according to real-time indoor loads [7]. This reduces temperature fluctuation ranges and extends fluctuation periods, significantly improving temperature control precision and thermal comfort. Studies show that variable-frequency air conditioners maintain stable control accuracy under high ambient temperatures, whereas temperature fluctuations of fixed-frequency units can increase to $\pm$2.0–3.0°C, enlarging the comfort gap between the two types [8]. With advantages of energy saving, low noise, and precise temperature control, variable-frequency air conditioners are widely used in scenarios requiring long-term continuous operation, high thermal comfort, or large load variations [9].

Both types of air conditioners exhibit temperature fluctuations after reaching the setpoint, with differing ranges depending on operation modes [10]. Fixed-frequency air conditioners typically cause fluctuations exceeding 2°C due to their working principle, while variable-frequency units limit fluctuations to within 1°C. Such fluctuations degrade both the energy efficiency of air conditioning systems and occupant thermal comfort [11]. Reducing steady-state temperature fluctuations after setpoint attainment has become an important research topic in air conditioning control. Existing solutions fall into three categories:

- Hardware upgrading: Optimizing core components such as compressors and throttling parts. Variable-frequency air conditioners equipped with DC inverters and electronic expansion valves can restrict steady-state fluctuations to $\pm$0.8–0.9°C [12]; precision air conditioners using modulated compressors and multi-sensor arrays achieve accuracy of $\pm$ 0.1–0.3°C [13]. However, hardware modification is impractical for residential applications.
- Operation mode optimization: Strategies including "rapid cooling and steady-state fine-tuning," upward air supply, and auxiliary circulation fans to balance indoor airflow without hardware

 doi:10.20944/preprints202605.1281.v1

changes [14,15]. These methods rely on manual operation and improve perceived comfort but do not fundamentally eliminate temperature fluctuations.

- Control algorithm optimization: Intelligent algorithms such as fuzzy neural network-based PID enhance adaptive control and mitigate disturbances from occupancy and solar radiation [16]; centralized air conditioners combined with load sensing and group control stabilize temperature and reduce energy consumption [17]. However, these algorithms require training data, have poor cross-building generalization, and depend on high-precision sensors and dedicated controllers, leading to high deployment costs [18,19].

To address the limitations of high hardware costs, manual intervention, and insufficient algorithm generalization, this paper proposes an adaptive air conditioning temperature control algorithm based on millimeter-wave radar sensing. The algorithm intelligently identifies the bed region using radar data and dynamically adjusts air speed and direction according to bed position to suppress steady-state fluctuations in the average indoor temperature.

Compared with existing methods, the proposed approach offers the following benefits: (1) Strong universality, without model training for specific building scenarios; (2) No modification to core air conditioning hardware, with low deployment barriers and controllable costs; (3) Fully automatic and unobtrusive adjustment, reducing user operation and improving overall thermal comfort.

2. Problem Statement

Although variable-frequency air conditioners have significantly reduced temperature fluctuations compared to fixed-frequency units, steady-state oscillations of the return air temperature T_1 after setpoint attainment remain a persistent issue in bedroom environments. Existing solutions—whether hardware upgrades, manual operation adjustments, or intelligent control algorithms—either incur prohibitive costs, rely on user intervention, or lack generalization across different room layouts [12–17]. More importantly, none of these approaches address the root cause of the problem: the spatial non-uniformity of airflow induced by the bed.

In a bedroom, the bed acts simultaneously as the largest obstacle and the most persistent heat source [20]. As an obstacle, it alters the propagation path and velocity distribution of the conditioned air, creating local recirculation zones and dead areas where the supply air cannot effectively reach the return vent. As a heat source, the human body generates a metabolic heat flux of approximately 40–50 $\mathrm{W/m^2}$ during rest, forming a stable thermal boundary layer around the bed surface [21]. Intermittent human movements (e.g., turning over, sitting up) further disturb this boundary layer, introducing transient thermal loads that are unpredictable to a conventional thermostat [21]. These dual effects cause the measured temperature T_1 to oscillate even when the compressor frequency is stable, because the air mixing near the indoor unit's sensor does not reflect the actual thermal state of the occupied zone.

Conventional air conditioning control relies solely on feedback from built-in temperature sensors and lacks spatial awareness—the system does not know where the bed is relative to the indoor unit. Consequently, it cannot determine whether the supplied air is being deflected by the bed or is actually reaching the occupant area. The controller may therefore take inappropriate actions, which often exacerbate overshoot and oscillation rather than suppress them.

To overcome this fundamental limitation, two interrelated technical problems must be solved:

1. **Non-intrusive bed localization** – How to accurately estimate the distance d and azimuth θ of the bed relative to the indoor unit using low-cost sensing that requires no hardware modification? This requires robust extraction of the bed position from sparse, noisy point cloud data while rejecting transient human activities and multipath reflections.
2. **Spatially aware steady-state control** – How to dynamically adjust air supply direction (louver angles) and fan speed using the estimated bed position together with real-time return air temperature and compressor operating parameters, so that the steady-state fluctuation of indoor temperature T_1 is suppressed to a level significantly below that of conventional variable-frequency

 doi:10.20944/preprints202605.1281.v1

systems? The proposed solution must generalize across different bedroom geometries without per-room model training.

This paper addresses these two problems by introducing a millimeter-wave radar-based bed localization algorithm and a LGBM weak teacher model trained on massive cloud data. The approach requires no hardware changes, operates fully automatically, and its effectiveness in suppressing T_1 fluctuations is validated on 719 real-world devices.

3. Methods

This study aims to identify the bed position using indoor temperature T_1 from built-in sensors and human activity tracking via millimeter-wave radar, obtaining distance and azimuth relative to the indoor unit. Based on multi-source sensing data, the system dynamically regulates air speed and direction to optimize airflow distribution toward the bed, eliminate interference from bed obstruction, and suppress periodic fluctuations of T_1 after setpoint attainment. To validate the strategy, a LGBM weak teacher model is constructed using massive cloud-measured datasets, and control parameters are optimized iteratively to minimize T_1 fluctuation, providing a technical solution for precise bedroom temperature control.

3.1. Bed Region Localization Algorithm Based on Millimeter-Wave Point Cloud Clustering

We begin by applying three sequential preprocessing steps to the raw millimeter-wave radar point cloud data, which contains noise, outliers, and redundant points irrelevant to bed localization [22,23].

3.1.1. Radar Point Cloud Data Preprocessing

Millimeter-wave radar generates large volumes of raw observation data containing noise, outliers, and redundant points irrelevant to bed localization [22]. The following three preprocessing steps are applied sequentially [23].

(1) Time Window Selection

During nighttime sleep (20:00–08:00), occupants remain recumbent for long periods, producing spatially concentrated point clouds with high signal-to-noise ratio. The time window is defined as:

$$T_{sleep} = \{t \mid h_t \geq 20 \cup h_t \leq 8\} \tag{1}$$

where, T_{sleep} is nighttime sleep time window, t is time and h_t is hour at time t.

Only records within this window are retained to suppress interference from daytime activities.

(2) Outlier Removal

(a) Two filtering rules are applied

Null value removal: Let d_t and θ_t denote the measured distance and azimuth at time t, respectively. Records with null values in either d_t or θ_t are discarded.

(b) Points with distance exceeding the maximum effective detection range ($d_{\max} = 5m$) are removed.

The validity condition is:

$$V(z_t) = V_1(z_t) \cdot V_2(z_t) \tag{2}$$

where, $V(z_t)$ is validity flag of radar point z_t (1 for valid), $V_1(z_t)$ is null value filtering rule, and $V_2(z_t)$ is out-of-range filtering rule. $V(z_t) = 1$ indicates a valid point.

The nighttime candidate point set is:

$$P_{bed} = \left\{ z_t = (d_t, \theta_t) \middle| V(z_t) = 1, t \in T_{sleep} \right\} \tag{3}$$

where, P_{bed} is nighttime bed candidate point set, d_t is distance of point z_t, and θ_t is azimuth of point z_t.

 doi:10.20944/preprints202605.1281.v1

(3) Coordinate Transformation

Valid points are converted from polar coordinates (d, θ) to 2D Cartesian coordinates (x_i, y_i) with the radar as the origin to facilitate Euclidean distance-based clustering [24].

3.1.2. Density-Based Clustering and Bed Position Estimation

The estimation of bed position follows a three-stage density-based procedure. First, the limitations of direct mean estimation are analyzed, demonstrating that simple coordinate averaging is vulnerable to out-of-bed events and noise points, thereby necessitating spatial clustering. Second, the principle of the density-based clustering algorithm is described, focusing on how a sliding window search identifies the cluster with maximum point density. Third, the final bed center is determined as the mean of points within the optimal cluster and then transformed back to polar coordinates $(d_{\text{bed}}, \theta_{\text{bed}})$, which provide essential spatial inputs for the subsequent LGBM control model.

Limitations of Direct Mean Estimation

Although preprocessed candidate points are generally valid, direct coordinate averaging is biased by occasional out-of-bed events (e.g., getting up at night) and noise points from multi-path reflection and clutter [25]. Such outliers shift the global mean, potentially causing localization errors larger than the bed width and leading to incorrect air direction control. Spatial clustering is therefore necessary to separate true bed points from noise and outliers.

Principle of Density-Based Clustering

This study adopts a density-based spatial clustering approach to process P_{bed}. The core idea is that the bed corresponds to the densest and most concentrated spatial cluster in the point cloud [26].

First, the initial centroid $(\bar{x}_0, \bar{y}_0)$ of all candidate points is calculated. An initial rectangular search window $\mathcal{W}_0$ with side length $L = 2m$ (matching typical bed dimensions) is centered at the centroid:

$$\mathcal{W}_0 = \left\{ (x, y) \; |x - \bar{x}_0| \leq \frac{L}{2}, \; |y - \bar{y}_0| \leq \frac{L}{2} \right\} \tag{4}$$

where, $\mathcal{W}_0$ is initial rectangular search window, $L = 2m$ is side length, and $(\bar{x}_0, \bar{y}_0)$ is the initial centroid of all candidate points.

The window is shifted in four directions by step $\delta = 0.5m$, generating five candidate windows. The point density ρ_k in each window $\mathcal{W}_k$ is counted. The optimal window k^* is the one with maximum density:

$$k^* = \arg\max_k \rho_k \tag{5}$$

where, k^* is optimal window index, and ρ_k is point density in window k.

If multiple windows have equal density, the one closest to the global centroid is selected to ensure stability [27]. The optimal cluster $\mathcal{C}_{bed}$ contains points within the best window.

Bed Position Identification and Output

The estimated bed center $(\hat{x}_{bed}, \hat{y}_{bed})$ is the mean coordinate of points in $\mathcal{C}_{bed}$. The center is converted back to polar coordinates to obtain radial distance d_{bed} and azimuth θ_{bed} relative to the indoor unit:

$$d_{bed} = \sqrt{\hat{x}_{bed}^2 + \hat{y}_{bed}^2} \tag{6}$$

$$\theta_{bed} = \arctan 2 \left(\hat{x}_{bed}, \hat{y}_{bed} \right) \tag{7}$$

where, d_{bed} is radial distance of bed center relative to indoor unit, and θ_{bed} is azimuth of bed center relative to indoor unit. The output $(d_{\text{bed}}, \theta_{\text{bed}})$ serves as a key input for the LGBM control model to guide precise air direction and speed regulation.

 doi:10.20944/preprints202605.1281.v1

3.1.3. Statistical Analysis and Evaluation Metrics for Distance/Angle Data

Evaluation Framework

Two metrics are used to quantify engineering feasibility: spatial dispersion (consistency and stability of estimates) and localization accuracy (agreement with ground truth). Minimum Enclosing Circle (MEC) radius and position accuracy are adopted as core indicators.

Minimum Enclosing Circle Radius

The MEC radius R_{MEC} is computed using Welzl's algorithm [28], which efficiently finds the smallest circle covering all points for a given device. Smaller R_{MEC} indicates higher spatial concentration and estimation stability.

Bed Position Accuracy

An error tolerance $\tau = 0.5m$ is set based on American Society of Heating, Refrigerating and Air-Conditioning Engineers (ASHRAE) standards and bed dimensions (double bed half-width $\geq 0.675m$), ensuring estimates remain within the bed surface [29].

The indicator function is:

$$1_j(\tau) = \begin{cases} 1, & R_{MEC,j} < \tau \\ 0, & R_{MEC,j} \geq \tau \end{cases} \tag{8}$$

where, $1_j(\tau)$ is indicator function for device j (1 for accurate localization), $R_{MEC,j}$ is minimum enclosing circle radius of device j, and τ is error tolerance (0.5 m).

System-wide accuracy is:

$$Acc(\tau) = \frac{1}{K}\sum_{j=1}^{K} 1_j(\tau) = \frac{\{\, j \mid R_{MEC,j} < \tau \}}{K} \tag{9}$$

Cumulative distribution of the minimum enclosing circle radius–systematically analyzing how the identification performance varies with the accuracy requirement, introducing the cumulative distribution function (CDF) of the minimum enclosing circle radius:

$$F(r) = \frac{\{\, j \mid R_{MEC,j} \leq r \}}{K}, \quad r \geq 0 \tag{10}$$

F(r) shows the proportion of devices with $R_{MEC,j} < r$, where $Acc(\tau) = F(\tau)$. Descriptive statistics including mean radius and linear trend between radius and point count are also analyzed [30].

3.2. Control Algorithm Principle

A lightweight LGBM weak teacher model is constructed to address the difficulty of suppressing average indoor temperature fluctuations after setpoint attainment using conventional control. By fusing bed position and air conditioning operational features, the model learns optimal air direction and speed regulation to minimize steady-state T_1 fluctuations and enhance thermal comfort.

LGBM is selected for the following reasons: Efficient histogram-based decision tree construction and Gradient-based One-Side Sampling (GOSS) reduce memory usage and accelerate training for large-scale cloud data; Support for multi-task learning enables simultaneous prediction of air direction and speed with good interpretability; obustness to heterogeneous features (distance, angle, temperature) matches multi-source fusion requirements.

3.2.1. Light Gradient Boosting Machine (LGBM)

LGBM improves upon Gradient Boosting Decision Tree (GBDT) with histogram algorithm and GOSS [31,32], greatly enhancing training efficiency for large datasets [33]. Its objective function is:

$$\mathcal{L}^{(t)} = \sum_{i=1}^{n} l(y_i, \hat{y}_i^{(t-1)} + f_t(x_i)) + \Omega(f_t) \tag{11}$$

 doi:10.20944/preprints202605.1281.v1

where $l(\cdot)$ is the loss function and $\Omega(\cdot)$ is a regularization term to prevent overfitting [34–36].

3.2.2. LGBM Model for Air Conditioning Control

The model is trained on approximately 105,000 cloud records including radar data, indoor temperature, setpoint temperature, compressor frequency, and return air temperature T_1. It preserves user setpoints and only optimizes air direction and speed to stabilize T_1.

Input Feature Space

The model takes five-dimensional features:

$$\mathcal{X} = \{d, \theta, T_1, f, \triangle T_{set}\} \tag{12}$$

where, d is radial distance (0–5 m), θ is azimuth (30–150°), T_1 is real-time return air temperature (°C), f is compressor frequency (0–100), and $\triangle T_{set} = |T_1 - T_{set}^{raw}|$ is temperature deviation (°C); $\triangle T_{set} < 0.5\,^{\circ}\mathrm{C}$ indicates setpoint attainment.

Features are standardized to eliminate scale effects.

Output Space

Outputs preserve T_{set} and predict control parameters:

$$\mathcal{Y} = \left\{T_{set}, D_{big}, D_{small}, V\right\} \tag{13}$$

where, D_{big} is left/right large louver (binary), D_{small} is left/right small louver (binary), and V is fan speed (6 classes: 1–5 fixed, 6 auto).

Multi-Task Loss Function

A weighted loss prioritizes T_1 fluctuation minimization:

$$\mathcal{L}_{weak} = \omega_{fluc} L_{fluc} + \left(1 - \omega_{fluc}\right)\left(\omega_{big} L_{cls}^{big} + \omega_{small} L_{cls}^{small} + \omega_{wind} L_{cls}^{wind}\right) \tag{14}$$

where, $\omega_{fluc} = 0.7$ is weight of fluctuation loss, L_{fluc} is fluctuation loss, $\omega_{big} = 0.4$ is weight of large louver classification loss, L_{cls}^{big} is large louver classification loss, $\omega_{small} = 0.3$ is weight of small louver classification loss, L_{cls}^{small} is small louver classification loss, $\omega_{wind} = 0.3$ is weight of fan speed classification loss, L_{cls}^{wind} is fan speed classification loss.

The core fluctuation loss is:

$$L_{fluc} = \frac{1}{N_{reach}} \sum_{i=1}^{N_{reach}} \left|T_{1,i} - T_{set,i}^{raw}\right| \tag{15}$$

where, L_{fluc} is core fluctuation loss, N_{reach} is number of samples reaching setpoint, $T_{1,i}$ is return air temperature of sample i, and $T_{set,i}^{raw}$ is original set temperature of sample i. Classification losses use cross-entropy.

Self-Supervised Consistency Regularization

To improve robustness to feature noise, consistency regularization is added:

$$\mathcal{L}_{consist} = \mathcal{L}_{consist}^{feat} + \mathcal{L}_{consist}^{fluc} \tag{16}$$

where, $\mathcal{L}_{consist}$ is self-supervised consistency regularization loss, $\mathcal{L}_{consist}^{feat}$ is feature consistency loss, and $\mathcal{L}_{consist}^{fluc}$ is fluctuation consistency loss.

Final loss:

$$\mathcal{L}_{weak}^{final} = \mathcal{L}_{weak} + \lambda_{consist} \mathcal{L}_{consist} \tag{17}$$

 doi:10.20944/preprints202605.1281.v1

where $\lambda_{consist} = 0.1$ is the regularization weight, used to balance the objectives of minimizing fluctuations and optimizing model robustness.

3.2.3. Model Training and Hyperparameters

The dataset is split 7 : 3 for training and validation. Early stopping is applied if validation loss does not improve for 10 consecutive iterations. Key hyperparameters are listed in Table 1.

Table 1. Core Hyperparameters of the Model.

Sub-Module	Number of Decision Trees	Maximum Tree Depth	Learning Rate	Regularization Coefficient λ	Regularization Coefficient γ
Large louver classification sub-model	100	6	0.05	0.01	0.1
Small louver classification sub-model	100	6	0.05	0.01	0.1
Fan speed classification sub-model	90	6	0.05	0.01	0.1

Model Evaluation Metrics

Model evaluation metrics are divided into core metrics and auxiliary metrics. Core metrics are about Mean absolute fluctuation, variance and no fluctuation ratio. Auxiliary metrics are about accuracy and F1-score.

(1) Core metrics

(a) Mean Absolute Fluctuation (MAF_{T_1}):

$$MAF_{T_1} = \frac{1}{N_{reach}} \sum_{i=1}^{N_{reach}} \left| T_{1,i} - T_{set,i}^{raw} \right| \tag{18}$$

where MAF_{T_1} is mean absolute fluctuation of return air temperature; N_{reach} is number of samples reaching setpoint;

(b) Variance(VAR_{T_1}):

$$VAR_{T_1} = \frac{1}{N_{reach}} \sum_{i=1}^{N_{reach}} (T_{1,i} - T_{set,i}^{raw})^2 \tag{19}$$

where VAR_{T_1} is variance of return air temperature;

(c) No Fluctuation Ratio (NFR_{T_1}):

$$NFR_{T_1} = \frac{\left| \left\{ i \mid \left| T_{1,i} - T_{set,i}^{raw} \right| < 0.1\,^{\circ}\mathrm{C} \right\} \right|}{N_{reach}} \tag{20}$$

where NFR_{T_1} is no fluctuation ratio of return air temperature;

(2) Auxiliary metrics

(a) Accuracy:

$$Accuracy = \frac{1}{N_{cloud}} \sum_{i=1}^{N_{cloud}} \mathbb{I}\left(\hat{y}_i^{weak} = y_i^{cloud} \right) \tag{21}$$

where Accuracy is model classification accuracy; N_{cloud} is number of cloud samples; y_i^{weak} is predicted label of weak teacher model for sample i; y_i^{cloud} is true label of cloud sample i.

 doi:10.20944/preprints202605.1281.v1

(b) $F1_{score}$:

$$F1 = \frac{2 \times Precision \times Recall}{Precision + Recall} \tag{22}$$

where F1 is $F1_{score}$; Precision is precision rate; Recall is recall rate.

4. Results

4.1. Radar Localization

4.1.1. Single-Device Localization Results

Figure 2 presents the bed localization pipeline for a typical device, including polar coordinate point distribution and Cartesian MEC results. Valid nighttime points are highly concentrated in azimuth 60–70° and distance 0.2–0.4 m. The MEC center is (0.78, 1.74) with $R_{mec} = 0.177m$, providing a stable bed position estimate.

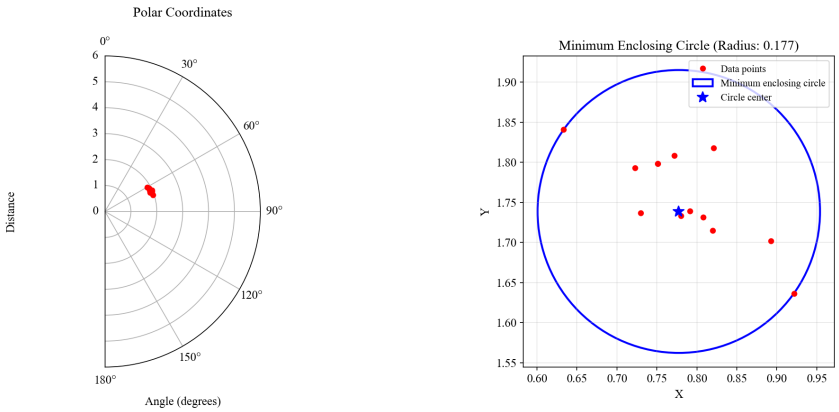

Figure 2. Bed position identification result of a single device.

4.1.2. Statistical Results on the Full Dataset

A total of 719 devices were processed for batch evaluation.Radius distribution: RMEC follows a unimodal right-skewed distribution concentrated in 0.1–0.5 m, with mean 0.323 m and median 0.308 m; Boxplot: The interquartile range lies below τ=0.5 m, confirming high consistency for most devices;CDF: F(0.5)=0.836, indicating 83.6% of devices meet the 0.5 m accuracy requirement; Radius vs. point count: The trend $\widehat{R}_{MEC} = 0.013 \cdot N + 0.213$ shows a mild increase with sample size, with most points classified as accurate (green).

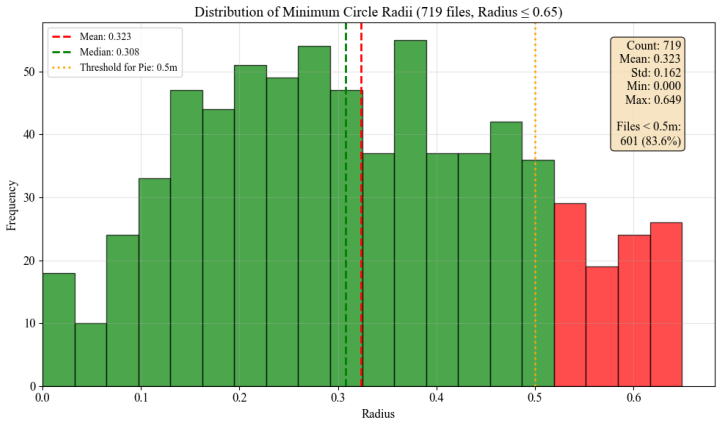

Figure 3. Distribution histogram of the minimum enclosing circle radius.

 doi:10.20944/preprints202605.1281.v1

4.1.3. Accuracy Evaluation

At $\tau = 0.5m$, 601 of 719 devices are classified as accurate, yielding a system localization accuracy of 83.6%. The result demonstrates reliable generalization in real-world scenarios and sufficient precision for subsequent air control.

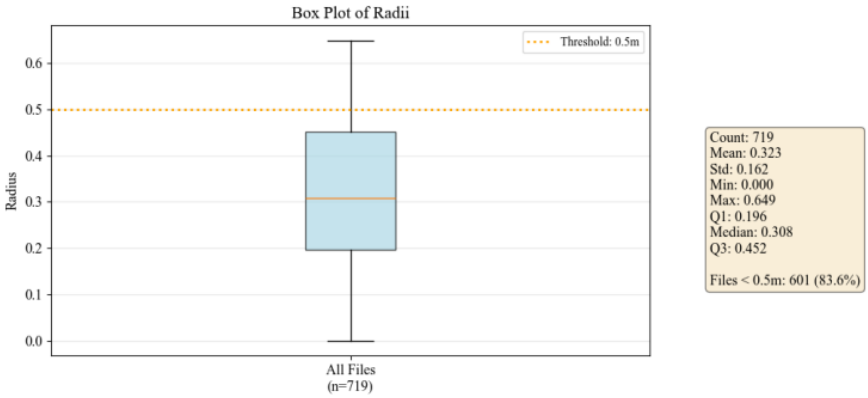

Figure 4. Boxplot of the minimum enclosing circle radius.

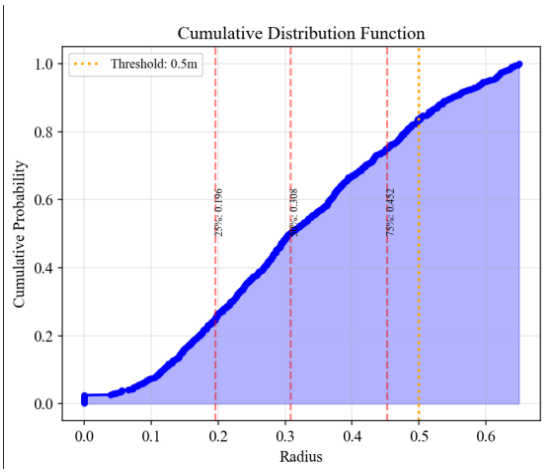

Figure 5. Cumulative distribution function of the minimum enclosing circle radius.

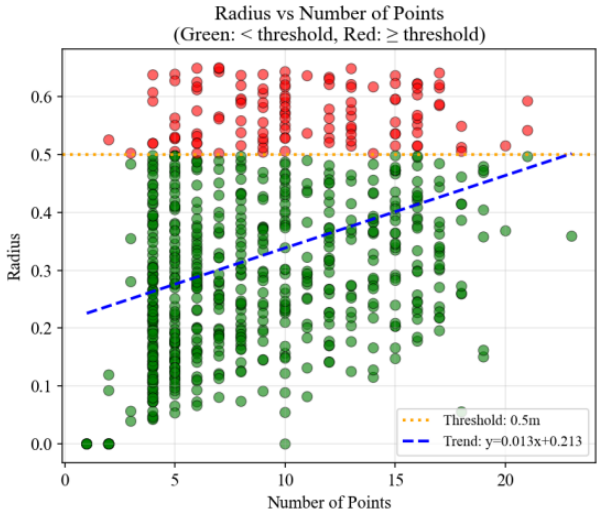

Figure 6. Relationship between the minimum enclosing circle radius and the number of candidate-points.

 doi:10.20944/preprints202605.1281.v1

4.2. Air Conditioning Control Algorithm Results

4.2.1. Model Convergence Analysis

The training and validation loss curves converge smoothly without significant overfitting, verifying effective learning of feature–control mappings and good generalization. Early stopping optimizes computational efficiency.

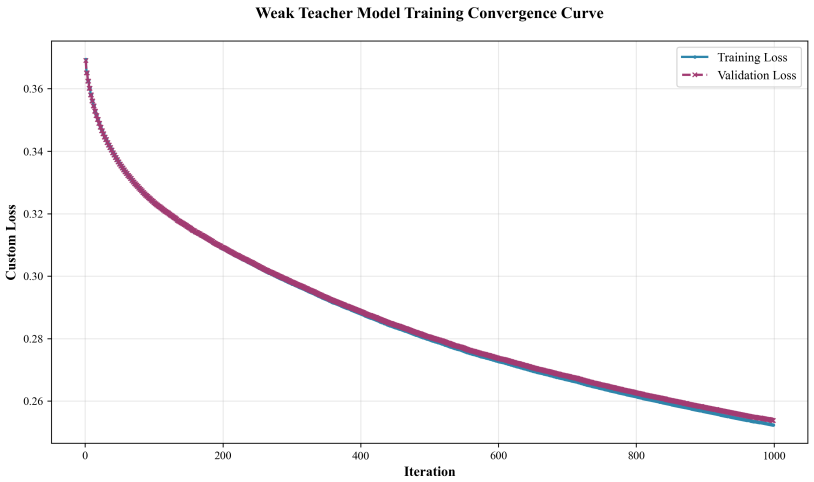

Figure 7. Training convergence curve of the weak teacher model.

4.2.2. Feature Importance Analysis

Feature importance ranking reveals:

1. Azimuth θ is the dominant feature. It determines the spatial position of the bed relative to the indoor unit, which directly affects airflow organization and temperature distribution. The model adjusts airflow direction based on azimuth to improve uniformity and stabilize T_1 after the setpoint is reached.
2. Radial distance d is the second-most important feature. It determines the required air supply intensity: higher speed ensures full coverage for distant areas, while lower speed avoids local discomfort and temperature instability for nearby areas.
3. Real-time temperature T_1 ranks third. It reflects the current indoor thermal state and guides control strategy: gentle airflow maintains stability near the setpoint, while active regulation corrects large deviations rapidly.
4. Temperature deviation ΔT_{set} and compressor frequency f play supporting roles. The former identifies the steady-state condition, and the latter indicates the real-time system load.

 doi:10.20944/preprints202605.1281.v1

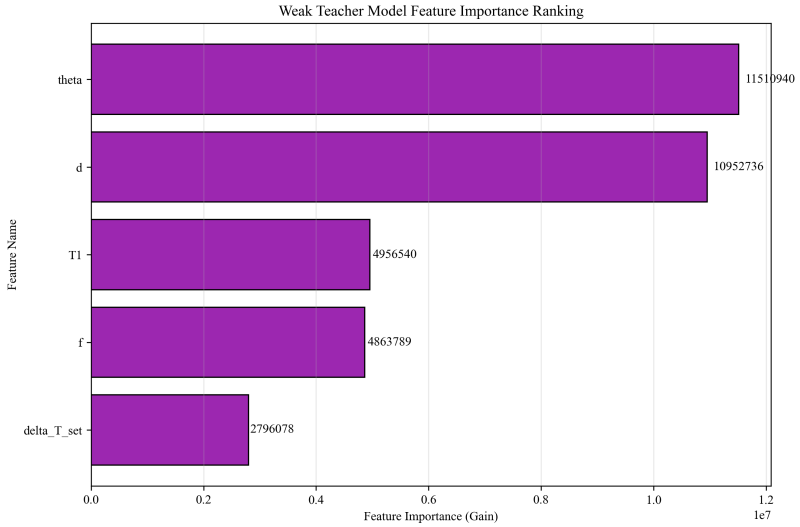

Figure 8. Feature importance ranking of the weak teacher model.

These results demonstrate that stable T_1 control after reaching the setpoint depends on accurate perception of the bed position and real-time thermal state, allowing the model to generate optimal air direction and speed regulation.

4.2.3. Core Fluctuation Metric Analysis

On validation set samples at setpoint attainment, MAF_{T_1} is 0.21°C, VAR_{T_1} is 0.064 °C^2, and NFR_{T_1} is 21.6%. T_1 is stably controlled within approximately ±0.2°C of the setpoint, with most fluctuations below 0.5°C, representing a substantial improvement over conventional fixed- and variable-frequency systems.

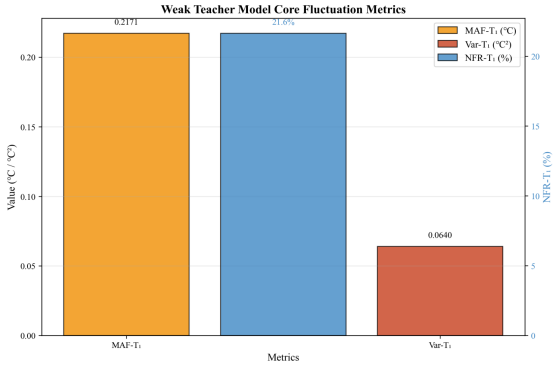

Figure 9. Core fluctuation metrics of the weak teacher model.

4.2.4. Auxiliary Metric Analysis

As shown in the figure, the accuracy and F1 of small louvers are about 0.99, the accuracy and F1 of large louvers are about 0.99, the accuracy of fan speed is 0.74, and the F1 of fan speed is 0.72.

 doi:10.20944/preprints202605.1281.v1

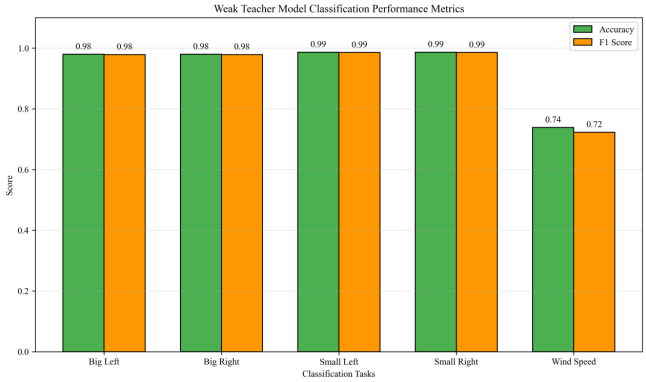

Figure 10. Auxiliary evaluation metrics of the weak teacher model.

High precision for louver control confirms reliable airflow regulation. Slightly lower speed performance reflects real-world complexity but still captures dominant patterns for practical deployment.

5. Discussion

This study proposes a temperature control algorithm based on millimeter-wave radar sensing and an LGBM weak teacher model to reduce steady-state fluctuations in average indoor temperature T_1 after setpoint attainment. Experimental results verify the feasibility and performance of the proposed method.

For bed localization, the pipeline combines nighttime filtering, outlier removal, density-based clustering, and MEC evaluation. On 719 devices, the mean R_{MEC} is 0.323 m, with 83.6% accuracy at 0.5 m tolerance. The estimated bed position provides critical spatial input for stabilizing T_1.

For control modeling, feature importance confirms the dominant role of spatial information, which conventional temperature-only control lacks. By incorporating bed position, the system reduces MAF_{T_1} to 0.21°C with variance 0.064 °C^2, outperforming fixed-frequency (±2–3°C) and standard variable-frequency (≈ ±1 °C) units. The multi-task framework and consistency regularization ensure reliable and physically consistent outputs.

Compared with existing solutions, the proposed method offers strong universality, low cost, and hands-free operation. Limitations include dependence on specific air conditioning hardware and reliance on bed position as the sole spatial feature. Future work may explore multi-object separation, multi-region spatial fusion, and integration of additional environmental features.

6. Conclusions

This paper addresses excessive temperature fluctuations in air-conditioned rooms after setpoint attainment by introducing a smart control algorithm combining millimeter-wave radar sensing and a weak teacher model. The system identifies bed location as a key spatial feature affecting airflow distribution and uses an LGBM model trained on large-scale cloud data to optimize louver position and fan speed, minimizing T_1 fluctuations.

The bed localization algorithm achieves 83.6% accuracy across 719 devices under a 0.5 m error tolerance. The LGBM control model yields stable convergence, with spatial features as primary decision inputs. It reduces steady-state MAF_{T_1} to 0.21°C and Var_{T_1} to 0.064 °C^2, with louver control $F1_{scores}$ above 0.98 and fan speed $F1_{score}$ of 0.72, supporting real-world deployment.

This work integrates spatial sensing and machine learning to provide a low-cost, highly versatile approach for improving temperature stability in residential air conditioning. Future research will focus on multi-spatial-feature fusion control and extended environmental inputs to further enhance performance.

Abbreviations

 doi:10.20944/preprints202605.1281.v1

The following abbreviations are used in this manuscript :

Abbreviation	Full Form
LGBM	Light Gradient Boosting Machine
MEC	Minimum Enclosing Circle
CDF	Cumulative Distribution Function
ASHRAE	American Society of Heating, Refrigerating and Air-Conditioning Engineers
PID	Proportional-Integral-Derivative
GOSS	Gradient-based One-side Sampling
GBDT	Gradient Boosting Decision Tree
MAF	Mean Absolute Fluctuation
NFR	No Fluctuation Ratio

References

1. Handbook, A. Fundamentals atlanta: American society of heating, air-conditioning and refrigeration engineers. *Inc* **2009**.
2. Pérez-Lombard, L.; Ortiz, J.; Pout, C. A review on buildings energy consumption information. *Energy and buildings* **2008**, *40*, 394–398.
3. Lan, L.; Wargocki, P.; Lian, Z. Quantitative measurement of productivity loss due to thermal discomfort. *Energy and Buildings* **2011**, *43*, 1057–1062.
4. Saidur, R.; Masjuki, H.H.; Jamaluddin, M. An application of energy and exergy analysis in residential sector of Malaysia. *Energy policy* **2007**, *35*, 1050–1063.
5. Wang, S.; Ma, Z. Supervisory and optimal control of building HVAC systems: A review. *Hvac&R Research* **2008**, *14*, 3–32.
6. Yu, F.; Chan, K. Economic benefits of improved condenser features for air-cooled chillers serving an air-conditioned hotel. *Applied thermal engineering* **2006**, *26*, 1063–1073.
7. Nasution, H.; Wan Hassan, M.N. Potential electricity savings by variable speed control of compressor for air conditioning systems. *Clean Technologies and Environmental Policy* **2006**, *8*, 105–111.
8. Chen, Y.; Chan, Y.; Wei, C. A comparative study between a constant-speed air-conditioner and a variable-speed air-conditioner. *ASHRAE Transactions* **2009**, *115*, 326.
9. Fong, K.F.; Hanby, V.I.; Chow, T.T. HVAC system optimization for energy management by evolutionary programming. *Energy and buildings* **2006**, *38*, 220–231.
10. Xia, L.; Ma, Z.; Kokogiannakis, G.; Wang, S.; Gong, X. A model-based optimal control strategy for ground source heat pump systems with integrated solar photovoltaic thermal collectors. *Applied energy* **2018**, *228*, 1399–1412.
11. Dzyuban, Y.; Ching, G.N.; Yik, S.K.; Tan, A.J.; Banerjee, S.; Crank, P.J.; Chow, W.T. Outdoor thermal comfort research in transient conditions: A narrative literature review. *Landscape and Urban Planning* **2022**, *226*, 104496.
12. Choi, J.; Kim, Y. Capacity modulation of an inverter-driven multi-air conditioner using electronic expansion valves. *Energy* **2003**, *28*, 141–155.
13. Kosar, D.R.; Witte, M.J.; Shirey, D.B.; Hedrick, R.L. Dehumidification issues of Standard 62-1989. *ASHRAE journal* **1998**, *40*, 71–75.
14. Hoyt, T.; Arens, E.; Zhang, H. Extending air temperature setpoints: Simulated energy savings and design considerations for new and retrofit buildings. *Building and Environment* **2015**, *88*, 89–96.
15. Laskari, M.; de Masi, R.F.; Karatasou, S.; Santamouris, M.; Assimakopoulos, M.N. On the impact of user behaviour on heating energy consumption and indoor temperature in residential buildings. *Energy and Buildings* **2022**, *255*, 111657.
16. Dounis, A.I.; Caraiscos, C. Advanced control systems engineering for energy and comfort management in a building environment—A review. *Renewable and Sustainable Energy Reviews* **2009**, *13*, 1246–1261.
17. He, M.; Cai, W.J.; Li, S.Y. Multiple fuzzy model-based temperature predictive control for HVAC systems. *Information sciences* **2005**, *169*, 155–174.
18. Wang, S.; Xu, X. Optimal and robust control of outdoor ventilation airflow rate for improving energy efficiency and IAQ. *Building and Environment* **2004**, *39*, 763–773.
19. Gao, Y.; Ruan, Y.; Fang, C.; Yin, S. Deep learning and transfer learning models of energy consumption forecasting for a building with poor information data. *Energy and Buildings* **2020**, *223*, 110156.

 doi:10.20944/preprints202605.1281.v1

20. Huang, G.; Wang, S.; Xu, X. A robust model predictive control strategy for improving the control performance of air-conditioning systems. *Energy Conversion and Management* **2009**, *50*, 2650–2658.
21. Cheng, Y.; Niu, J.; Gao, N. Thermal comfort models: A review and numerical investigation. *Building and environment* **2012**, *47*, 13–22.
22. Xia, Z.; Ding, G.; Wang, H.; Xu, F. Person identification with millimeter-wave radar in realistic smart home scenarios. *IEEE Geoscience and Remote Sensing Letters* **2021**, *19*, 1–5.
23. Prabhakara, A.; Jin, T.; Das, A.; Bhatt, G.; Kumari, L.; Soltanaghai, E.; Bilmes, J.; Kumar, S.; Rowe, A. High resolution point clouds from mmwave radar. In Proceedings of the 2023 IEEE International Conference on Robotics and Automation (ICRA). IEEE, 2023, pp. 4135–4142.
24. Moon, J.; Kim, B.K.; Kang, J. Fixed point cloud normalization and none-sequential modeling for hand gesture recognition based on short-range mmwave radar sensor's sparse time-series point cloud. *IEEE Sensors Journal* **2024**, *24*, 10656–10668.
25. Yu, J.T.; Yen, L.; Tseng, P.H. mmWave radar-based hand gesture recognition using range-angle image. In Proceedings of the 2020 IEEE 91st Vehicular Technology Conference (VTC2020-Spring). IEEE, 2020, pp. 1–5.
26. El-Sonbaty, Y.; Ismail, M.A.; Farouk, M. An efficient density based clustering algorithm for large databases. In Proceedings of the 16th IEEE international conference on tools with artificial intelligence. IEEE, 2004, pp. 673–677.
27. Wang, T.; Ren, C.; Luo, Y.; Tian, J. NS-DBSCAN: A density-based clustering algorithm in network space. *ISPRS International Journal of Geo-Information* **2019**, *8*, 218.
28. Chrystal, G. On the problem to construct the minimum circle enclosing n given points in the plane. *Proceedings of the Edinburgh Mathematical Society* **1885**, *3*, 30–33.
29. Hart, R.; Myer, M.; Halverson, M.; Chen, Y.; Rosenberg, M.; Xie, Y.; Tyler, M.; Loper, S.; Zhang, J.; Poehlman, E. National Cost-Effectiveness of ANSI/ASHRAE/IES Standard **2020**.
30. Gärtner, B. Fast and robust smallest enclosing balls. In Proceedings of the European symposium on algorithms. Springer, 1999, pp. 325–338.
31. Hastie, T.; Tibshirani, R.; Friedman, J.H.; Friedman, J.H. *The elements of statistical learning: data mining, inference, and prediction*; Vol. 2, Springer, 2009.
32. Chen, T.; Guestrin, C. Xgboost: A scalable tree boosting system. In Proceedings of the Proceedings of the 22nd acm sigkdd international conference on knowledge discovery and data mining, 2016, pp. 785–794.
33. Ke, G.; Meng, Q.; Finley, T.; Wang, T.; Chen, W.; Ma, W.; Ye, Q.; Liu, T.Y. Lightgbm: A highly efficient gradient boosting decision tree. *Advances in neural information processing systems* **2017**, *30*.
34. Bishop, C.M.; Nasrabadi, N.M. *Pattern recognition and machine learning*; Vol. 4, Springer, 2006.
35. Bühlmann, P.; Hothorn, T. Boosting algorithms: Regularization, prediction and model fitting **2007**.
36. Natekin, A.; Knoll, A. Gradient boosting machines, a tutorial. *Frontiers in neurorobotics* **2013**, *7*, 63623.